SAND99-1381J

GROWTH OF ORIENTED C11$_b$ $MoSi_2$ BICRYSTALS USING A MODIFIED CZOCHRALSKI TECHNIQUE

J. D. Garrett[1], P. Peralta[2†], J. R. Michael[3], F. Chu[4], K. J. McClellan[4] and T. E. Mitchell[4]

1. McMaster University, Brockhouse Institute for Materials Research, Hamilton, Ontario, L8S 4M1, CANADA.

2. Arizona State University, Department of Mechanical and Aerospace Engineering, P.O. Box 876106, Tempe, AZ 85287-6106.

3. Sandia National Laboratory, Mail Stop 1405, Albuquerque, NM 87185.

4. Materials Science and Technology Division, MS K765, Los Alamos National Laboratory, Los Alamos, NM 87545.

ABSTRACT

Oriented bicrystals of pure C11$_b$ $MoSi_2$ have been grown in a tri-arc furnace using the Czochralski technique. Two single crystal seeds were used to initiate the growth. Each seed had the orientation intended for one of the grains of the bicrystals, which resulted in a 60° twist boundary on the (110) plane. Seeds were attached to a water-cooled seed rod, which was pulled at 120 mm/h with the seed rod rotating at 45 rpm. The water-cooled copper hearth was counter-rotated at 160 rpm. Asymmetric growth ridges associated with each seed crystal were observed during growth and confirmed the existence of a bicrystal. It was also found that careful alignment of the seeds was needed to keep the grain boundary from growing out of the boule. The resulting boundary was characterized by imaging and crystallographic techniques in a scanning electron microscope. The boundary was found to be fairly sharp and the misorientation between the grains remained within 2° from the misorientation between the seeds.

---

† Corresponding author. Phone: +1-602-965-2849, Fax: +1-602-965-1384, e-mail: pperalta@asu.edu.

PACS Codes: 81.10.F, 61.72.M

Keywords: Silicide, Bicrystal, Crystal Growth, Grain Boundary.

INTRODUCTION

Molybdenum disilicide ($MoSi_2$) has the tetragonal $C11_b$ structure and is a promising material for high temperature structural applications due to its high oxidation resistance, low density compared to nickel superalloys and high specific stiffness [1]. These advantages are, however, hindered by its poor low temperature fracture toughness. Numerous studies have been carried out using single crystals and polycrystals in an attempt to understand the reasons for this behavior. These studies found that $MoSi_2$ has 5 independent slip systems and that single crystals exhibit dislocation plasticity, in compression, at room temperature and below [2-4]; however, polycrystals are brittle up to 1,000 °C [1], indicating that this material has a "grain boundary problem." Unfortunately, single crystal studies cannot address grain boundary effects, and polycrystalline studies do not allow one to isolate the local behavior at a given grain boundary to determine the specific interactions between grains. Testing of bicrystal specimens would take advantage of all the knowledge gained in single crystal research, and the presence of a single grain boundary would make it possible to isolate phenomena such as strain localization, slip transmission, intergranular fracture, crack transmission across the interface, solute segregation, etc., all in a well controlled system. In order to realize this goal, bicrystal samples with controlled orientations need to be prepared in a reliable and reproducible manner. Bridgman techniques have been used to grow bicrystals of intermetallics (NiAl) using double seeds [5], using an alumina mold. Unfortunately, the high melting temperature of $MoSi_2$ (2020 °C) makes using molds quite difficult and expensive, since contamination of melt is quite difficult to avoid. This article describes the procedures

used to grow oriented $MoSi_2$ bicrystals from the melt using a double seed and the Czochralski technique in a Tri-Arc furnace with a water-cooled copper hearth. These bicrystals will be used to study the effects of boundaries on the mechanical properties of $MoSi_2$.

EXPERIMENTAL

The $MoSi_2$ single crystals used to prepare the seeds were grown using the optical floating zone technique [6]. The desired crystallographic directions required for each seed were found using the back reflection Laue technique and rectangular parallelepipeds with dimensions 2 x 5 x 5 mm^3 were cut using a precision diamond saw. The geometry and the crystallography of the seeds used are shown in Fig. 1. The boundary is on the (110) plane common to both seeds and the growth was along the <111> direction. This crystallographic orientation corresponds to a 60° rotation about [110] of one seed with respect to the other, i.e., the bicrystal should have a 60° twist boundary on the (110) plane. This misorientation was chosen because the growth and two lateral directions are crystallographically equivalent for the two seeds. This is expected to produce stable grain boundaries. Both grains should show the same growth behavior in these directions.

The two seeds were silver-soldered to the flat end of the water-cooled seed rod keeping the two (110) planes together and aligning the lateral edges. Proper alignment of the seeds in both vertical and horizontal planes was difficult to achieve, since positioning the seeds on the flat end of the rod while soldering resulted in some tilt of the <111> axes of the seeds with respect to the growth direction.

The bicrystals were grown in a Centorr Tri-Arc furnace, similar to that described in [7]. This technique was chosen because it has been used to grow single crystals of

$MoSi_2$ with great success [4]. The furnace was powered with a 300 A arc welding power supply, using two arcs with a total current of 125 A.

High purity, chemically cleaned Mo and Si were arc-melted to obtain approximately 10 gr. of polycrystalline $MoSi_2$ with 2 at.% excess Si, to compensate for evaporation of this element during crystal growth.

The polycrystalline material was melted in the Tri-Arc furnace using a water-cooled copper hearth, after evacuating and purging the chamber with high purity Ar at least three times, and leaving a constant flow of gettered Ar into the chamber which was vented at a slight positive pressure by using a relief valve. The melt was allowed to stabilize and the hearth was rotated at 160 rpm. The water-cooled seed rod was counter-rotated at 45 rpm. The double seed was slowly brought in contact with the molten material and was kept in touch with the melt for a few minutes in order to achieve a smooth solid-liquid interface and to round the corners of the rectangular seeds. The seed rod was then pulled at a rate of approximately 120 mm/h. An outline of the growth setup is shown in Fig. 2. The growth process was observed with a telescope through a welding glass shield.

The growth was stopped when either the melt was too small or after one of the arcs extinguished. The resulting boule was retrieved from the chamber and the double seed was recovered by breaking it off the boule. The same seeds were used two more times, while trying to improve their alignment on the seed rod.

The fracture surfaces of the samples were examined in a JEOL 6300 FX SEM operating at 15 kV. In addition, back reflection Laue technique was used to determine the orientation of each grain and the position of the boundary on the fracture surface. The same technique was used to cut two samples parallel to the (001) plane of one grain, which corresponds to the $(1\bar{1}2)$ plane of the other grain. These two samples were

a few millimeters apart along the axis of one bicrystal and they were polished to a finish of 1 μm diamond paste, so that they could be examined in the SEM. The sample closer to the seed was labeled 1 and the second sample, a few millimeters farther from the seeds, was labeled 2. The same samples were used to obtain electron backscattering (EBS) patterns of the two grains in each sample. These patterns were collected as follows. The samples were mounted at a tilt of 70.5° in a JEOL 6400 SEM equipped with a LaB_6 electron source. The instrument was operated at 20 kV with a beam current of about 5 nA. Patterns were recorded using a CCD-based detector that has been described previously [8]. Typical exposure times were 5 seconds. The patterns were indexed using software developed at Sandia National Laboratories, which automatically identifies the phase and also calculates an orientation matrix with respect to the microscope reference frame.

RESULTS AND DISCUSSION

Bicrystal Growth

Only two bicrystals were obtained out of the three attempts using the same double seed. Observation of the growth process revealed that bicrystals with the orientation used here developed two growth ridges, one on each grain, on opposite sides of the crystal. The presence of these two growth ridges could be used to identify the presence of two grains, since a crystal grown along a <111> direction, that resulted from one failed attempt to grow a bicrystal, only had one growth ridge. It was found that the misalignment of the seeds affected the development of the growth ridges, since one of them, always the one associated with the seed that was tilted away from the melt, would curve and finally disappear towards the surface of the boule, as shown

schematically in Fig. 3. This behavior was interpreted as the boule having two grains initially, with one of them becoming smaller as the growth progressed, until the larger grain dominated. The longest bicrystal (approximately 1.5 cm) was obtained for the best alignment of the seeds that could be obtained, which was still a few degrees away from the vertical direction. The growth ridges observed in this case are shown in Fig. 4, for the two sides of the bicrystal. Note that one growth ridge disappeared (Fig. 4b), suggesting that one grain had finally dominated. This was verified through observations on the fracture surfaces and cross-sectional samples.

Fracture surfaces

A typical fracture surface on the bicrystals is shown in Fig. 5. There were two areas that could be clearly differentiated. In one grain the fracture was on the (001) plane, as expected, since this is the cleavage plane [6, 9]. This corresponds to the region with a larger area ("large grain") in Fig. 5. There was a step separating the two regions, which corresponds to the grain boundary, and then the fracture morphology changed, since there were serrations on the other grain, which are parallel to the (001) plane for that grain. The presence of a relatively flat fracture surface in one grain and a serrated one in the other suggests that the large grain fractured first along the cleavage plane and the fracture plane deviated towards the (001) plane of the other grain once the crack hit the boundary.

Laue patterns for each region of the fracture surface were taken with the growth axis approximately parallel to the X-ray beam. Note in Fig. 5 that the longitudinal direction for both grains is close to <111>, as expected.

SEM of polished samples

The two polished samples were cut from the same bicrystals shown in Fig. 5, such that (001) was parallel to the surface of the large grain, whereas $(1\bar{1}2)$ was the corresponding surface in the other grain. The two samples are shown in Fig. 6. The sample close to the double seed (sample 1) is shown in Fig. 6a, and sample 2, taken from a location farther from the seeds, is shown in Fig. 6b. Arrows indicate the position of the grain boundary. It was found that cracks were already present in the samples, probably as a result of the removal of the seeds or due to the sample preparation technique.

Each sample showed two distinct regions, as can be seen in Fig. 6. One region was large and mostly free of cracks and other features and it corresponds to the (001) plane in the large grain. There was a crack present on that grain in both samples, close to the grain boundary and running approximately parallel to it. The second region corresponds to the smaller grain, where a series of cracks perpendicular to the interface were present. The fracture plane for these cracks is parallel to (001).

It was thought that the cracks on the large grain were in the boundary; however, a careful examination of both samples showed that these cracks did not run along the grain boundary, even for regions that were heavily cracked, as can be seen in Fig. 7. Note that the cracks in the smaller grain ran into the grain boundary and penetrated it; nevertheless, the grain boundary remained intact in between those excursions, which suggests that the grain boundary obtained using this procedure is stronger than the cleavage plane of this material.

Crystallographic Analysis

A region around the grain boundary relatively free of cracks was located in each sample using the SEM and EBS patterns were obtained at both sides of the interface, as

shown in Fig. 8, where both the image of the region selected in sample 1 and the indexed patterns are shown. Note that the boundary seems to be sharp, given the magnification and the contrast between the two grains. EBS patterns were obtained in each grain from locations as close as possible to the interface and then towards the bulk of each grain at 5-7 μm intervals; the patterns did not change. The patterns shown in Fig. 8 are representative of those obtained in each grain. The same was done in sample 2 with similar results.

The software used to index the patterns obtains the rotation tensor that relates the principal axes of the crystal structure and the directions parallel to the local coordinate system used. The matrices that describe this rotation for the grains of each sample are the following:

$$\mathbf{R}^{(1)}_{small} = \begin{bmatrix} 0.6114 & 0.7909 & -0.0271 \\ -0.3779 & 0.3219 & 0.8681 \\ 0.695 & -0.5204 & 0.4961 \end{bmatrix} \quad \mathbf{R}^{(1)}_{large} = \begin{bmatrix} 0.6923 & 0.7132 & -0.1102 \\ -0.7173 & 0.6968 & 0.0034 \\ 0.0791 & 0.0766 & 0.9939 \end{bmatrix} \quad (1)$$

$$\mathbf{R}^{(2)}_{small} = \begin{bmatrix} 0.6083 & 0.7836 & -0.1266 \\ -0.2921 & 0.3691 & 0.8823 \\ 0.7379 & -0.4996 & 0.4538 \end{bmatrix} \quad \mathbf{R}^{(2)}_{large} = \begin{bmatrix} 0.7372 & 0.6522 & -0.1766 \\ -0.6552 & 0.7538 & 0.049 \\ 0.1649 & 0.0795 & 0.9831 \end{bmatrix} \quad (2)$$

The third row of these matrices is the normal to the sample. The first row corresponds to the crystallographic direction that is perpendicular to this normal and to the electron beam. The second row is just a direction perpendicular to the other two. Note that the first two rows of the matrices corresponding to each grain are different for the two samples, which is due to the fact that the specimens were oriented differently with respect to the coordinate system used. The third rows for both large grains are within 10° from (001), as expected. Similarly, the third rows for both small grains are within 10° from $(1\bar{1}2)$, as it should be given the misorientation between the grains.

The tensor describing the misorientation between the two grains can be calculated using these matrices as follows [10]:

$$\mathbf{R}_{sl}^{(\kappa)} = (\mathbf{R}_{small}^{(\kappa)})^{-1}\mathbf{R}_{large}^{(\kappa)} \quad \kappa=1,2 \tag{3}$$

The only real eigenvector of each $\mathbf{R}_{sl}^{(\kappa)}$ is the axis common to both structures [10]. For sample 1, the common axis is $[0.7075, 0.7062, 0.0286]^T$. This is 1.64° away from <110>. The common axis for sample 2, which was located farther from the seeds than sample 1, is $[0.7156, 0.6984, 0.0105]^T$, and this is 0.92° away from <110>. Similarly, the trace of each $\mathbf{R}_{sl}^{(\kappa)}$ can be used to obtain the angle of rotation about the axis common to the two grains [10]. That angle is equal to 60.11° in sample 1 and 59.24° in sample 2. The misorientation was designed to result in a 60° twist boundary on the (110) plane and it can be seen that this is indeed the case of the resulting bicrystal, with less than two degrees of error. Note that the misorientation remains approximately unchanged as the distance from the double seed increases, which shows that the crystallographic directions chosen for the two seeds indeed resulted in a more stable interface as was assumed initially.

The fact that the boundary deviated from the vertical direction implies that the interface was no longer a twist boundary on the (110) plane. This is despite the fact that the misorientation between the grains was still the one for which the bicrystal was designed. Note that specifying the misorientation only fixes three of the five degrees of freedom required to describe a grain boundary [10], the other two being those required to identify the normal to the boundary plane. This normal is somewhat independent of the misorientation. The authors believe that the deviation of the boundary produced

thermal residual stresses during growth that contributed to form the cracks found in the sample. Further characterization of the grain boundary plane is underway.

CONCLUSIONS

Pure $MoSi_2$ bicrystals with selected twin boundaries can be grown from the melt using conventional Czochralski techniques.

The boundaries obtained corresponded to intended misorientation within 2° for both the axis and the angle of rotation. The misorientation remained relatively stable along the length of the bicrystal.

Alignment of the seeds with respect to the growth direction was not critical on obtaining bicrystals, but it was found that a good alignment results in longer bicrystals that can be then cut to obtain several samples from one growth.

The boundary obtained from this procedure was relatively sharp and no subgrains could be detected in its vicinity. In addition, cracks impinging at the interface resulted in transgranular fracture in the adjacent grain, suggesting that the boundary itself was stronger than the cleavage plane of the material.

ACKNOWLEDGMENTS

This research was supported by the Department of Energy, Office of Basic Energy Science, the Brockhouse Institute for Materials Research at McMaster University that provided the single crystal growth facilities, a postdoctoral fellowship to P. Peralta at Los Alamos National Laboratory and start-up funding to P. Peralta from the College of Engineering and Applied Science at Arizona State University. JRM acknowledges the support of the U. S. Department of Energy under contract #DE-AC04-94AL8500.

Sandia is a multiprogram Laboratory operated by Sandia Corporation, a Lockheed Martin Company, for the United States Department of Energy.

REFERENCES

1. Petrovic, J. J. (1995) *Mat. Sci. Eng.*, **A192/193**, 31-37.

2. Maloy, S. A., Heuer, A. H., Lewandowski, J. J. and Mitchell, T. E. (1992) *Acta metall. mater.*, **40**, 3159-3165.

3. Ito, K., Inui, H., Shirai, Y. and Yamaguchi, M. (1995) *Phil. Mag. A*, **72**, 1075-1097.

4. Maloy, S. A., Mitchell, T. E. and Heuer, A. H. (1995) *Acta metall. mater.*, 43, 657-668.

5. LeBleu, J. B., Mei, P. R., Levit, V. I. and Kaufman, M. J. (1998) *Scripta mater.*, 38, 415-422.

6. Peralta, P., Maloy, S. A., Chu, F., Petrovic, J. J. and Mitchell, T. E. (1997) *Scripta mater.*, **37**, 1599-1604.

7. Reed, T. B. and Pollard, E. R. (1968) *J. Crystal Growth*, **2**, 243-247.

8. Goehner, R. P. and Michael, J. R. (1996) *J. Research Nat. Institute of Standards and Technology*, **101**, 301-308.

9. Waghmare, U. V_t, Kaxiras, E., Bulatov, V. V. and Duesbery, M. S. (1998) *Mod. Sim. Mat. Sci. Eng.*, **6**, 493-506.

10. Sutton, A. P. and Ballufi, R. W. (1995) *Interfaces in Crystalline Materials*. New York: Oxford University Press.

Figure Captions

Fig. 1. Geometry and crystallography of the $MoSi_2$ seeds used to grow the bicrystal.

Fig. 2. Setup of the tri-arc furnace for bicrystal growth.

Fig. 3. Outline of the effect of seed misalignment on growth ridges.

Fig. 4. Growth ridges observed in the longest bicrystal obtained. (a) Side with the dominant grain; (b) Opposite side. The ridges are indicated by arrows.

Fig. 5. Fracture surface of a $MoSi_2$ bicrystal with a 60° twist boundary about [110]. The arrows in the Laue patterns show crystallographically equivalent poles in both grains. The pole towards the center of the pattern at the intersection of two major zone axes is parallel to <111>.

Fig. 6. (a) Cross section of the bicrystal close to the initial fracture surface (sample 1); (b) Cross section of the bicrystal a few millimeters farther from the seeds (sample 2).

Fig. 7. Grain boundary in a heavily cracked region in sample 1, imaged in the SEM.

Fig. 8. Region around the grain boundary of sample 1 and the EBS patterns obtained at each grain.

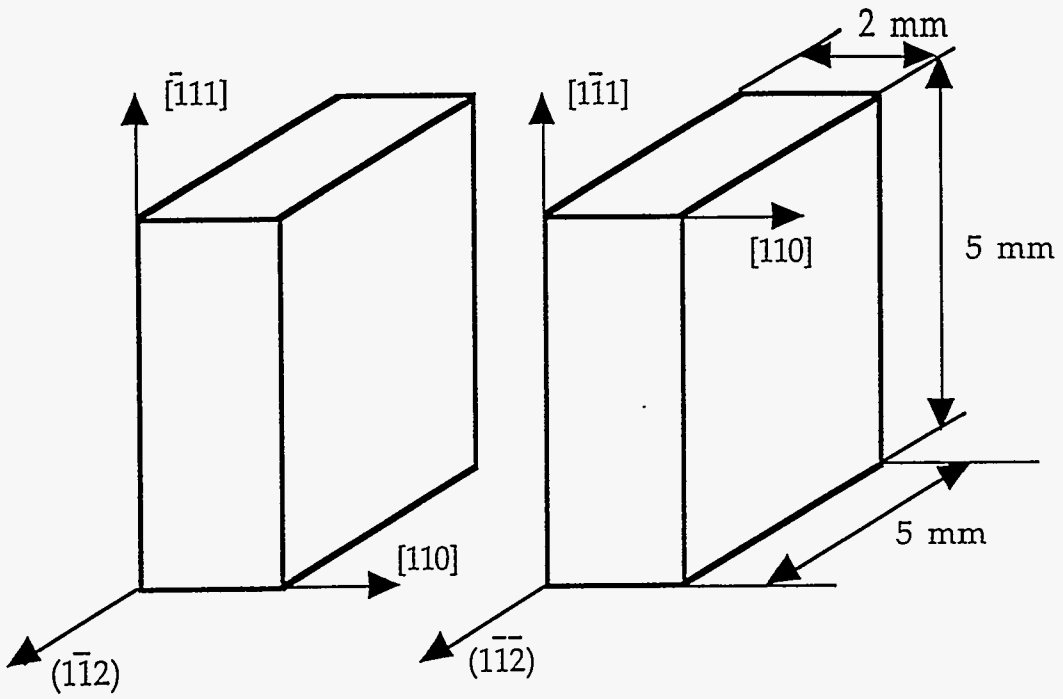

Fig. 1. Geometry and crystallography of the $MoSi_2$ seeds used to grow the bicrystal.

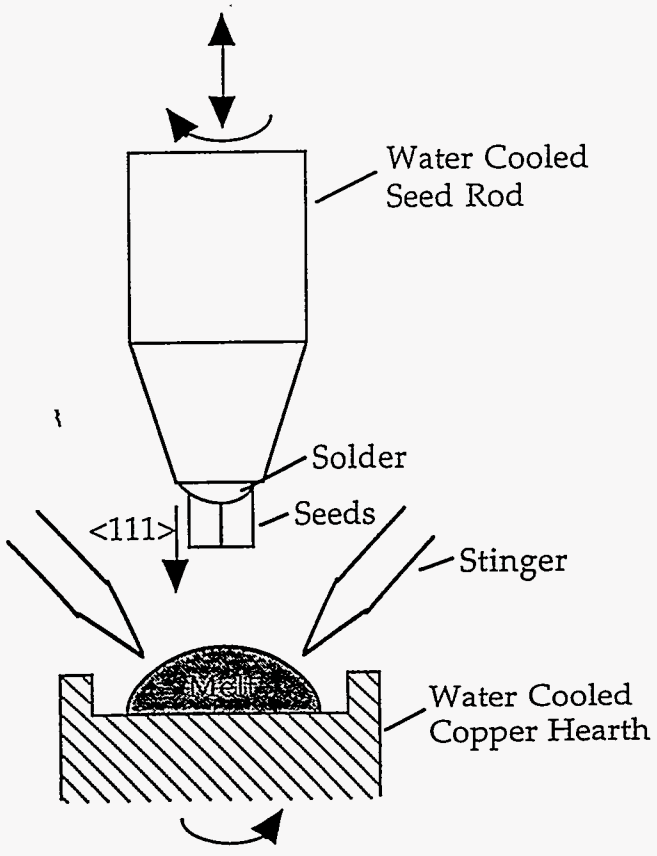

Fig. 2. Setup of the tri-arc furnace for bicrystal growth.

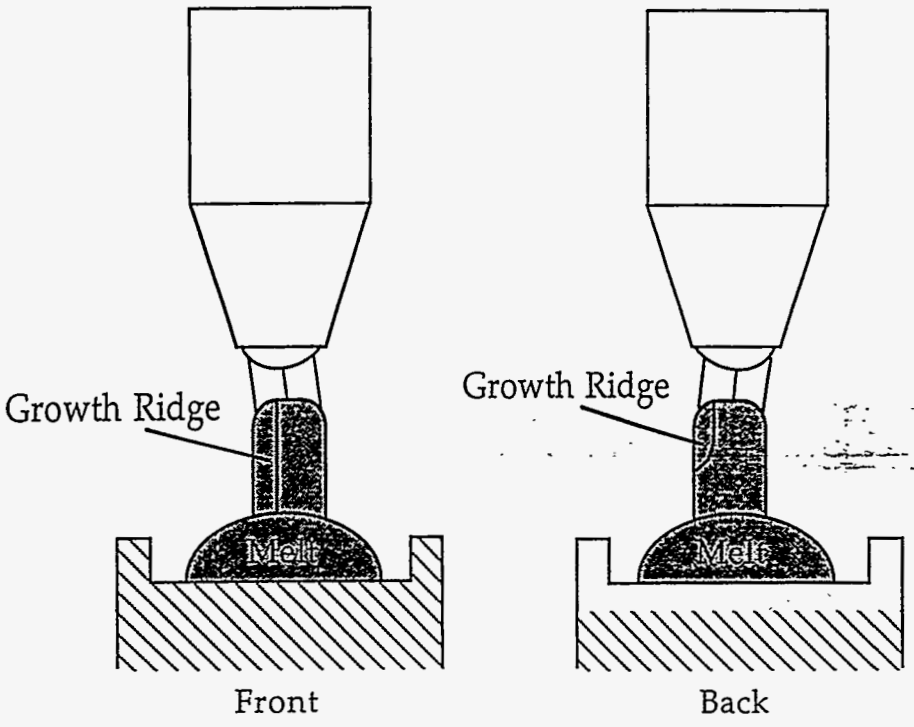

Fig. 3. Effect of seed misalignment on growth ridges.

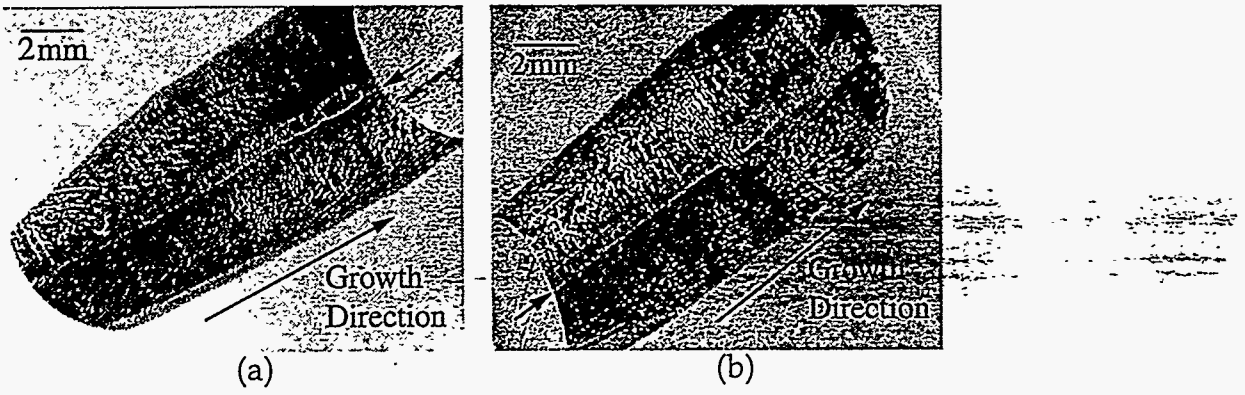

Fig. 4. Growth ridges observed in the longest bicrystal obtained. (a) Side with the dominant grain; (b) Opposite side. The ridges are indicated by arrows

Fig. 5. Fracture surface of a $MoSi_2$ bicrystal with a 60° twist boundary about [110]. The arrows in the Laue patterns show crystallographically equivalent poles in both grains. The pole towards the center of the pattern at the intersection of two major zone axes is parallel to <111>.

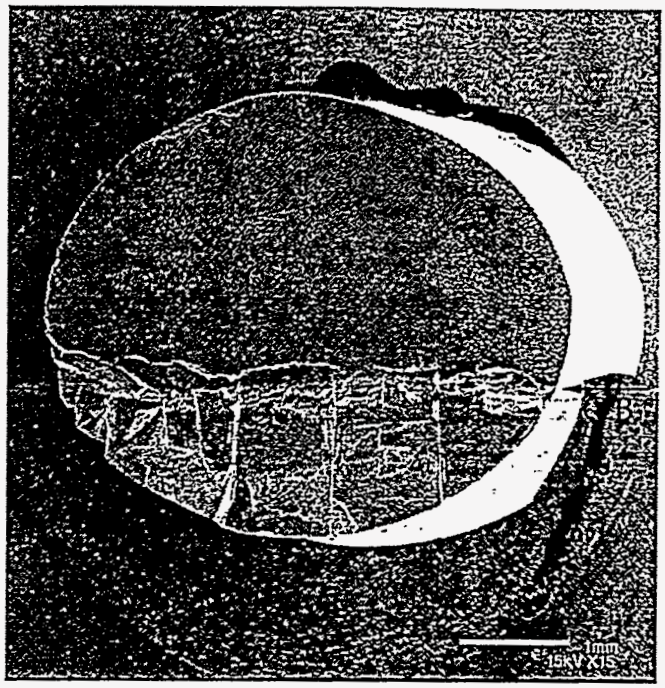

(a)

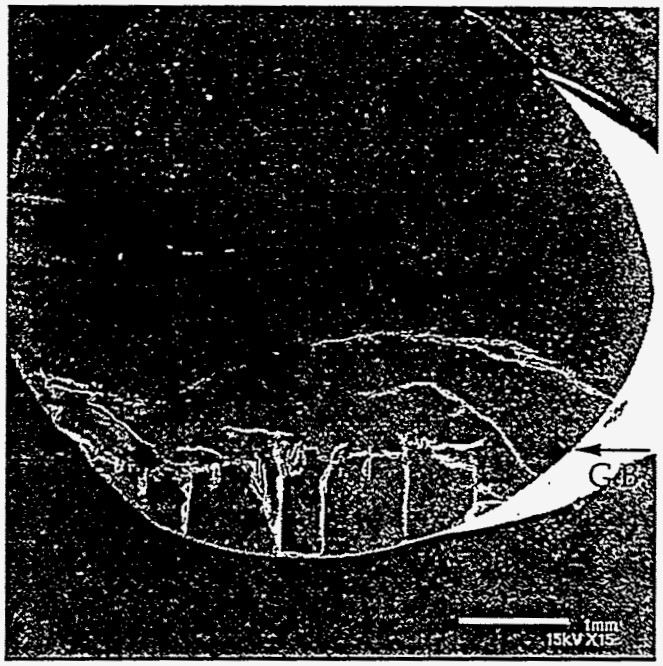

(b)

Fig. 6. (a) Cross section of the bicrystal close to the initial fracture surface (sample 1); (b) Cross section of the bicrystal a few millimeters farther from the seeds (sample 2).

(large) 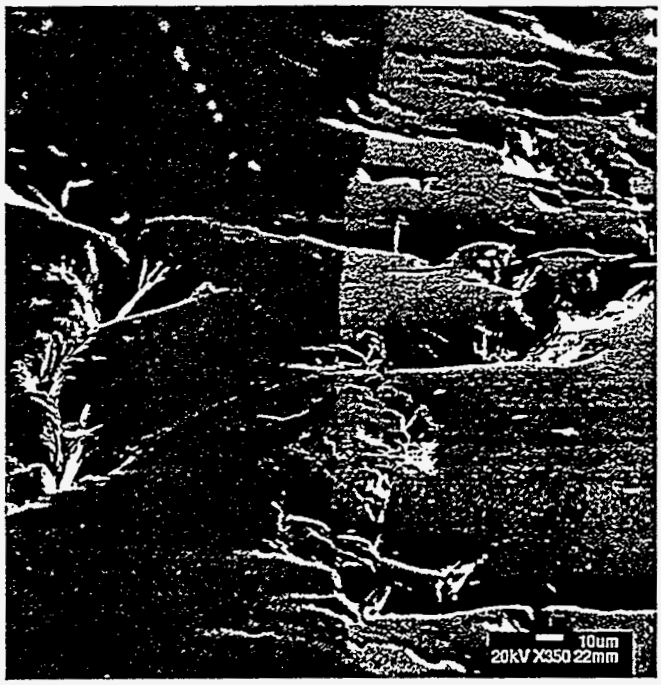

(small)

Fig. 7. Grain boundary in a heavily cracked region in sample 1, imaged in the SEM.

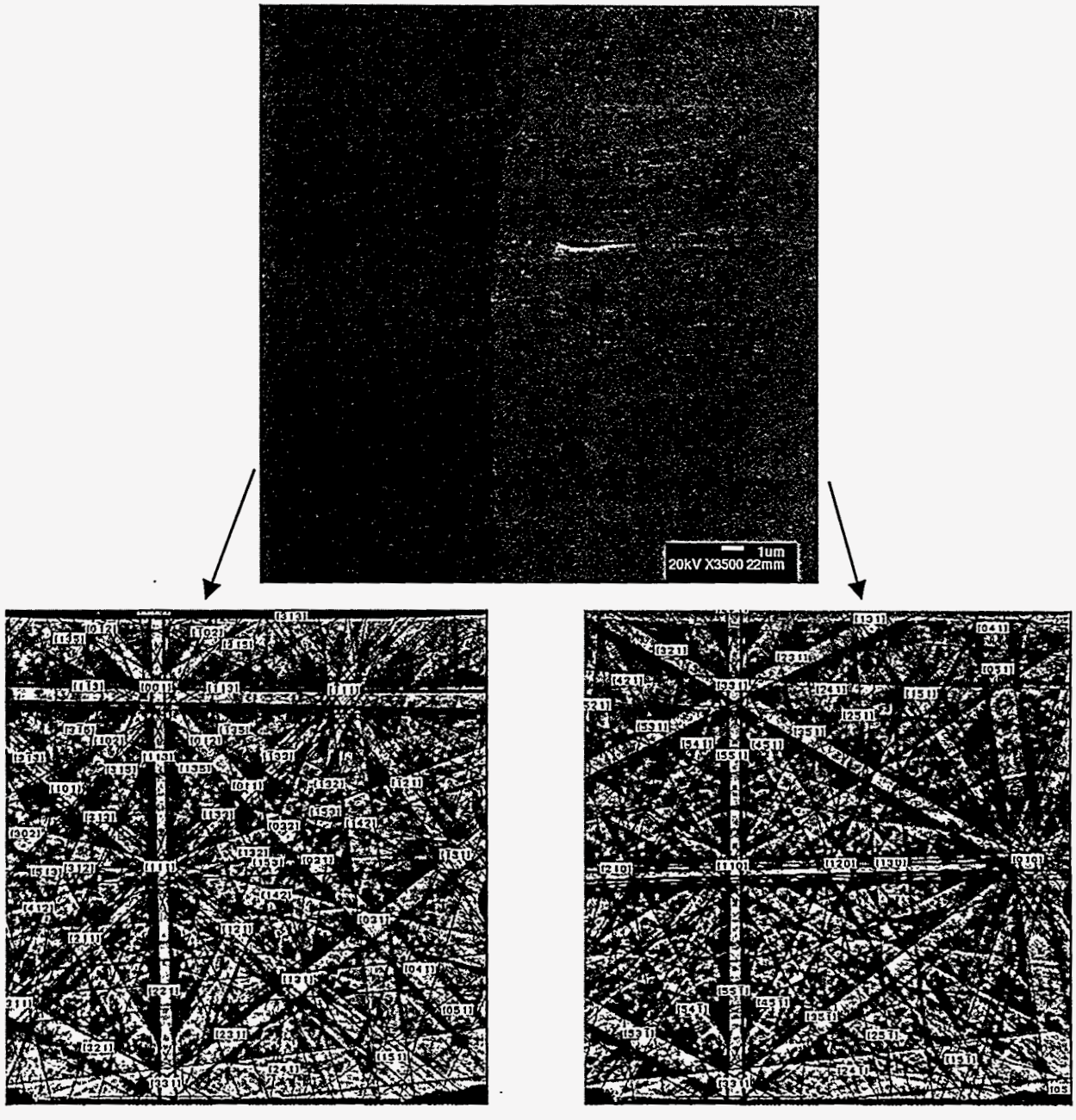

Fig. 8. Region around the grain boundary of sample 1 and the EBS patterns obtained at each grain.